International Research Journal of Engineering and Technology (IRJET) e-ISSN: 2395-0056
Volume: 11 Issue: 08 | Aug 2024 www.irjet.net p-ISSN: 2395-0072

DESIGN AND DEVELOPMENT OF RESOLVER BASED PMSM MOTOR CONTROLLER

Prashantha Naik K P
Department of Electrical and Electronics Engineering
RV College of engineering
Banglore,India

Dr S G Srivani
Department of Electrical and Electronics Engineering
RV College of Engineering
Bengaluru, India

K Akhilesh Reddy
Takumi motion control Pvt. Ltd
Bangalore,India

Ashwin H N
Takumi motion control Pvt. Ltd
Bangalore, India

***Abstract*— This paper presents the design and development of a resolver-based Permanent Magnet Synchronous Motor (PMSM) controller for electric vehicle applications. Nowadays, internal combustion (IC) engines are increasingly being replaced by plug-in hybrid, hybrid, or electric vehicles due to their disadvantages. In electric vehicles, the system comprises various components, including the Motor Control Unit (MCU), Intelligent Vehicle Control Unit (iVCU), Battery Management System (BMS), Fault Diagnostics Unit, and PMSM. This paper focuses primarily on the Motor Control Unit, which includes the control board, gate driver board, capacitor bank, and power board. Resolvers and encoders are utilized to measure the speed, position, and direction of the motor shaft. This feedback is used to adjust the power delivered to the motor, ensuring desired operating characteristics. Resolvers are preferred over encoders for harsh environments with high temperatures or radiation. A microcontroller generates PWM pulses to drive the inverter circuit and operate the PMSM motor**.

Keywords—PPMS motor, fly back converter, LT spice, op-amp, PMIC IC.

I. INTRODUCTION

Electric vehicles (EVs) were first invented in the early 19th century, around the 1820s and 1830s. They became economically viable in the 1890s. Despite their potential, EVs were initially less popular due to higher costs, lower speed ranges, and shorter distances compared to internal combustion engines (ICEs), which dominated the 20th century [1]. By the early 21st century, interest shifted towards EVs due to the environmental impact of ICEs, including carbon emissions, climate change, environmental damage, and adverse effects on human health [2].

Since 2010, global sales of electric vehicles have surged, reaching one million by September 2016. By the end of 2019, there were 4.8 million EVs in use, and it was projected that 10 million EVs would be sold by the end of 2020. This growth reflects the evolution of electric vehicles [3]-[6]. Compared to other motor types such as DC motors, synchronous motors, and induction motors, Permanent Magnet Synchronous Motors (PMSMs) offer superior performance, including better dynamic and steady-state characteristics, higher efficiency, reduced size, increased torque, and higher power density. These advantages lead to smaller motor sizes and fewer torque ripples during commutation [7]-[10]. PMSMs are widely used in defense, agriculture, and everyday applications due to the rapid development of power electronics.

PMSMs can be controlled using two primary methods: vector control and direct torque control. Vector control involves managing and measuring the stator current vector to control motor torque by generating excitation and torque currents based on the field-oriented principle [8]-[12]. Direct torque control directly regulates the torque [13]. In alternating current machines, such as induction or AC motors, torque creation is similar to that of direct current motors. The stator generates fields, and the rotor is not perpendicular. Field-Oriented Control (FOC) decouples flux and torque components, offering several advantages over the V/F control approach [14]-[18]:

1. Provides full torque across a wide range of speeds.
2. Improved dynamic performance.
3. Effective transient and steady-state analysis.
4. High torque and low current during starting.
5. Enhanced efficiency.

6. Decoupling of torque and current (flux) control.
7. Four-quadrant operation.

The primary goal of the resolver is to accurately calibrate or position the rotor in a Permanent Magnet Synchronous Motor (PMSM), which is crucial for field-oriented control [19]-[21]. This study focuses on how the resolver influences the output voltage of the sine and cosine waves generated using the two-winding technique [22]-[23]. The resolver's error, which affects the accuracy of the sine and cosine voltage signals, can lead to decreased electromagnetic force and impact the motor current due to rotor position inaccuracies. These errors can result in increased vibration and noise in the electrical drive system. The comparative study highlights that resolver errors contribute to motor vibration, and the experimental results validate the theoretical analysis of the resolver's accuracy [24]-[25].

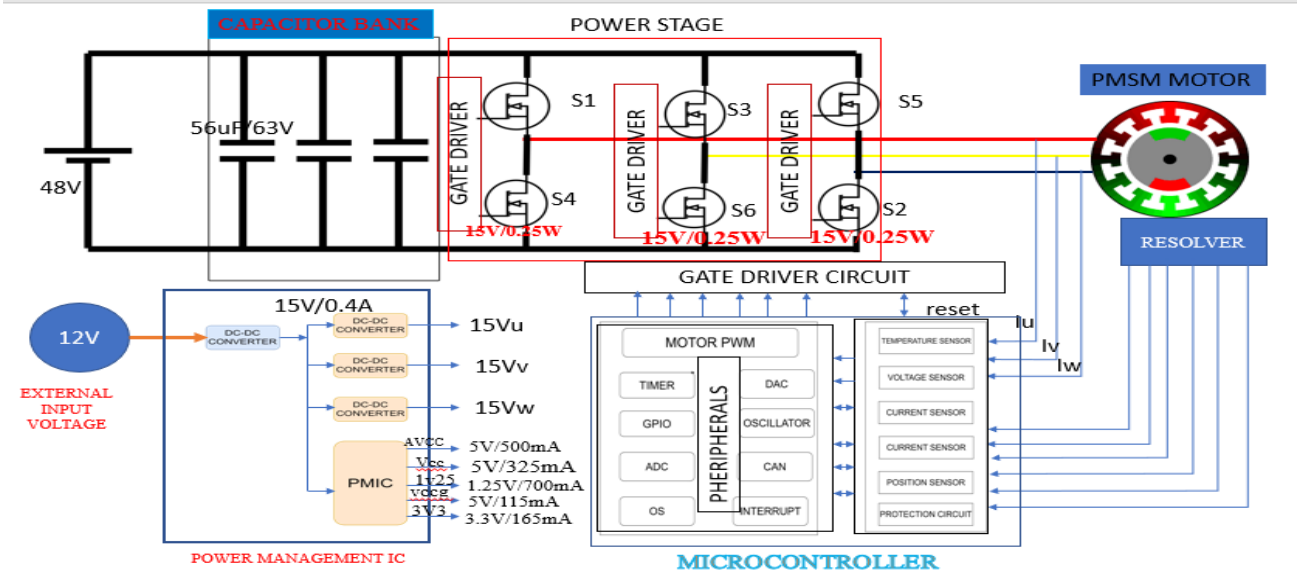

Fig 1 Block diagram of proposed system

II. PROPOSED APPROACH

A. *Block diagram*

An electric vehicle's various components include the on-board charge controller, DC-DC converter, power battery pack, auxiliary battery, intelligent vehicle control unit, motor control unit, battery management system, PMSM motor, telematics, and fault diagnostics unit. We're working on the motor controller unit (MCU), which is responsible for positioning the PMSM motor controller and powering the electrical vehicle. MCU consists of the following components: control board, gate driver board, capacitor bank, and inverter circuit (power stage) board. IAUT300N10S5N015 is a MOSFET IC with a rating of 100V, 300A, and 1.5mOhm that is used on the power stage board to convert constant DC voltage to pulsing AC, allowing the PMSM motor to work.

The NCU18WB473F6SRB thermistor IC is used to monitor resistance to temperature at various values and to protect the MOSFET from overheating. The LT8301 is a fly back power supply IC that creates and provides sufficient voltage to the gate driver IC. UCC27211 and UCC27524 ICs create pulses, which are subsequently fed to MOSFET ICs. We employ LMV842 voltage follower ICs in the power stage to measure phase and line voltages, which have an operating voltage of 5V and clip to 5V at higher voltages. The voltage follower circuit has a high input impedance and a low output impedance.

The LT8302 fly back auxiliary power supply ICs are used to produce a sufficient voltage of +15V from +12V for the voltage comparator or differential op-amp circuit, as well as supply voltage to the LT8301 power IC. Voltage comparator ICs compare two different voltage levels given to the microcontroller. This integrated circuit protects the MCU against overcurrent and overvoltage. The microcontroller runs at 3.3V and has a frequency of 240MHz. It offers two products: one with 252 pins for two motor controllers and the other with 176 pins for a single motor controller. A 144-pin microcontroller is used to operate a single motor.

The microprocessor generates pulses that are delivered to the gate driver circuit, which activates the inverter circuit. It also includes EEPROM memory, which is used to program languages. The microcontroller also has a Can trans receiver, which is

used to communicate with the motor and CPU. The resolver is utilized in the PMSM motor application to detect rotor position. Resolver hardware can be thought of as two inductive position sensors that generate two sinusoidal signals on output in response to a sinusoidal-shaped input signal. The amplitudes of the output signals fluctuate with the position of the shaft. The amplitude of one signal is proportional to the sine, whereas the other is proportional to the cosine of the shaft angle position.

In the power management section, the external input voltage of 12V is applied to the isolate fly back converter, which acts as a boost converter, converting the 12V supply to 15V. The converter's output voltage decides which circuits will be used: overcurrent amplifier, overvoltage amplifier, gate board, and power board circuit. The isolated fly back converter will receive the converter output at 15 volts. The 15V converter output voltage will be routed to two separate mosfet driver circuits, which will produce pulses independent of the inverter circuit switches. The power management integrated circuit applies a 15V input voltage from the converter output. The power management integrated circuit applies a 15V input voltage from the converter output. The PMIC has an adjustable frequency Buck/Boost pre-regulator with synchronous buck, three internal LDO watchdog timers, and a power-on reset. Its working voltage ranges between 2.8 and 36 volts. It features an adjustable synchronous buck regulator with a voltage of 1.25V and 700mA. The internal low-dropout regulators give output voltages of 5V/500mA, 5V/325mA, 5V/115mA, and 3.3V/165mA. The PMIC has a power on reset that is activated after a 15ms delay, and the microcontroller is reset using a fault flag.

B. Proposed topology

The suggested system uses a DC-DC converter that is based on a fly back converter. In the proposed system, two fly back DC-DC converters are used. The LT8302 will convert 12V to 15V, while another converter will convert 15V to 15V. These converters function similarly to the fly back converter topology depicted in Fig 2 below.

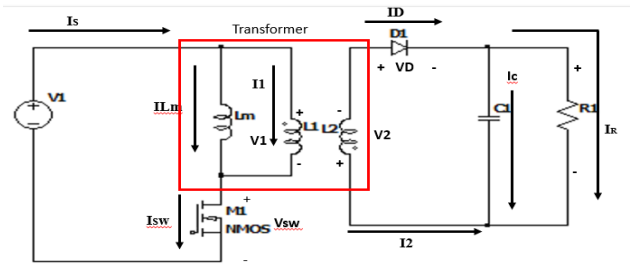

Fig 2 circuit diagram of the Fly back converter

The following assumptions are made for the flyback converter:

1. The initial components are ideal, such as the switch and diode.
2. The circuit is evaluated under steady-state conditions.
3. Large output capacitors prevent voltage ripples.
4. The switch will operate with a duty ratio of D, closed for DT and opened for (1-D) T.
5. Inductor current is continuous during continuous conduction mode (CCM).

Mode 1: The fly back converter works similarly to the Buck-Boost converter, with the only difference being voltage polarity. When the switch is closed, the secondary inductance of the transformer diode is turned off due to voltage polarity, so the current through the diode and the current flowing through the primary transformer are both zero. The supply voltage is directly connected to the transformer's magnetizing inductance, and the inductor charges using the supply voltage. The voltage across the diode will be less than zero, leading it to shut off. Because of the transformer's mutual inductance, the current flowing through the diode on the secondary side will be zero, resulting in a zero-primary current through the transformer. The power flow is presented in Fig 3.

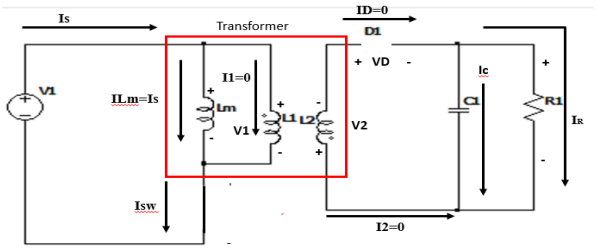

Fig 3 circuit diagram of the Fly back converter when switch is closed

Mode 2: The energy stored in the magnetizing inductor when the switch is closed; when the switch is open, the current flowing through the Lm does not change direction, so their voltage polarity changes, and the stored energy dissipates through the transformer's primary inductance, changing the dot polarity of the primary inductance. The current flows through the primary inductance, from undotted to dotted. The secondary side's mutual inductance causes the current to flow from dotted to undotted. When the polarity changes or current flows from the dotted to undotted terminals, the diode turns on. The energy was transferred to the capacitor and the load resistor. In this scenario, the capacitor will store energy. Figure 4 shows the circuit during switch open.

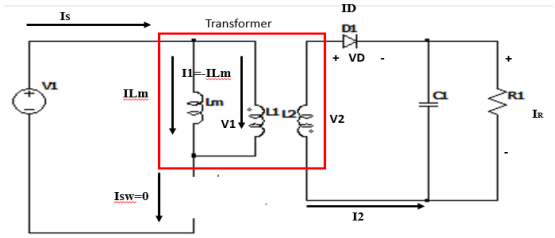

Fig 4 circuit diagram when switch ids open

III. SPECIFICATION AND DESIGN OF THE PROPOSED SYSTEM

A. *specification of the proposed system .*

The design specification of the proposed system and represented below in table I.

Table I specification of the proposed system

Parameter	Specification
Input Voltage Range	48V DC
Speed	6000 rpm
Efficiency	96%
Switching Frequency	10KHz
Motor	PMSM
Rotor type	Inner rotor
Auxiliary power supply	12V DC

B. *specification details of auxillary power supply*

Auxiliary power supply specification design details of the fly back converter follow below in Table 2.

Table II specification of the Fly back converter

Parameter	Specification
Input Voltage Range	12V DC
Output voltage	15V DC
Output current	400mA
Efficiency	85%
Load resistor	37.5Ohm
Topology	Fly back converter
Output power	6W
Reference voltage	1V DC

a. Select the transformer turns ratio calculation
Leakage voltage/Margin for transformer leakage spikes, Vleakage=24.25V

Output diode forward voltage, Vf=0.425V

$$Nps < \frac{65 - Vin(\max) - Vleakage}{Vout + Vf} \quad (1)$$

$$Nps < \frac{65 - 14 - 24.25}{15 + 0.425}$$

$$Nps < 1.67$$

Selection of turns ratio of the transformer, Nps=1

Primary and Secondary turns are, N1:N2=1:1

b. Calculation of the primary and secondary inductance

By calculating the primary and secondary inductance are used satisfy the minimum switch ON and OFF time of the switch is required,

$$Lpri \geq \frac{toff(\min) * Nps * (Vout + Vf)}{Isw(\min)} \quad (2)$$

$$Lpri \geq \frac{ton(\min) * Vin(\max)}{Isw(\min)}$$

$$Lpri \geq \frac{370 * 10^{-9} * 1 * (15 + 0.425)}{0.87}$$

$$Lpri \geq 9.655uH$$

$$Lpri = 10uH$$

Because of turns ration, Ns=1 hence the secondary inductance same as primary inductance,

$$Lsec = 10uH$$

c. Calculation of duty ratio for the switch
Duty ratio of the switch for the turn time or pulse width of the switch calculated below for the switch

$$D = \frac{(Vout + Vf) * Nps}{(Vout + Vf) * Nps + Vin} \quad (3)$$

$$D = \frac{(15 + 0.425) * 1}{(15 + 0.425) * 1 + 12}$$

$$D = 0.56 = 56\%$$

d. Calculation of switching current and switching frequency
The current flowing through the drain of the MOSFET switch which will reduces the EMI and voltage spikes of the transformer. Calculation of the switching current and switching frequency are shown below,

$$sw = \frac{Vout * Iout * 2}{\eta * Vin * D} \quad (4)$$

$$Isw = \frac{15 * 400 * 10^{-3} * 2}{0.85 * 12 * 0.56}$$

$$Isw = 2.09A$$

$$fsw = \frac{1}{ton + toff}$$

$$fsw = \frac{1}{\frac{Lpri * Isw}{Vin} + \frac{Lpri * Isw}{Nps * (Vout + Vf)}} \quad (5)$$

$$fs = \frac{1}{\frac{10*10^{-6}*2.09}{12} + \frac{10*10^{-6}*2.09}{1*(15+0.425)}}$$
$$\boldsymbol{fsw = 322.67kHz = 322kHz}$$

e. Calculation of the output diode current and reverse voltage of the output diode

The maximum current flowing through the output diode during the forward bias and maximum reverse withstand voltage for the diode during the reverse bias is calculated below,

$$Idiode = 0.6 * Isw(\max) * \text{Nps} \quad (6)$$
$$Idiode = 0.6 * 4.5 * 1$$
$$Idiode = 2.7A$$
$$Vreverse = Vout + \frac{Vin(\max)}{Nps} \quad (7)$$
$$Vreverse = 15 + \frac{15}{1}$$
$$Vreverse = 30V$$

f. Calculation of the output capacitor

By choosing the output capacitor to minimize the output ripple voltage of the Fly back converter by considering the increase in size and cost of a large capacitor. Output capacitor calculated for the output ripple less than ±1% calculated below,

$$Cout = \frac{Lpri*Isw^2}{2*Vout*\Delta Vout} \quad (8)$$
$$Cout = \frac{10*10^{-6}*4.5^2}{2*15*01}$$
$$Cout = 1.25*67.5*10^{-6} = 94.5uF$$

g. Calculation of snubber circuit and reverse voltage of Zener diode

The designing of the snubber circuit to reduce the EMI and leakage spikes voltage across the transformer and designing of the Zener diode for to withstand the maximum reverse voltage developed across the Zener diode during reverse bias is calculated below, the snubber circuit consists of resistor and capacitor connected in series.

$$Vzener(max) \leq 60 - \text{Vin}(\max) \quad (9)$$
$$Vzener \leq 60 - 15$$
$$Vzener \leq 45V$$

Designed values for snubber circuit given by R=39Ohm and C=470pF.

h. Select the reference resistor and feedback resistor

By choosing the proper values of the feedback resistor to minimize the output voltage regulation and the ratio of the feedback to reference resistor to maintain the 10kOhm. The following expression for calculating the feedback and reference resistors are given below,

$$Rfb = \frac{Rref*Nps*(Vout+Vf(T0))}{Vref} \quad (10)$$

By choosing Rref = 10kOhm.

$$Rfb = \frac{10*10^3*1*(15+0.425)}{1}$$
$$= 154.25$$
$$Rfb(new) = \frac{Vout}{Vout(measured)} * Rfb$$
$$= \frac{15*10*10^3}{15.14}$$
$$= 150.59kOhm$$
$$Rfb(new) = 150kOhm \quad (11)$$

i. Selection of Rtc resistor based on output voltage temperature variation

Calculation of the output voltage consisting of the output current and input voltage across the operating temperature condition calculated below,

$$-\frac{\delta Vf}{\delta T} = \frac{Vout(T1)-Vout(T2)}{T1-T2} \quad (12)$$
$$Rtc = \frac{3.35mV/C}{-\frac{\delta Vf}{\delta T}} \frac{Rfb}{Nps}$$
$$Rtc = \frac{3.35*10^{-3}*154*10^3}{1.48*10^{-3}*1} = 190kOhm$$

j. Calculation and selection of EN/UVLO resistor

Calculation of amount of hysteresis voltage required to select the values for R1 and R2 for UVLO. For UVLO pin the minimum voltage is 0.3V and less than 0.3V than IC's shutdown. The calculation of R1 and R2 is given below,

$$Vh = Vin(uvlo+) - Vin(uvlo-) \quad (13)$$

Let's considering Vin(uvlo+) =7.7V and Vin(uvlo-)=5.8V

Hysteresis voltage, $Vh = 7.7 - 5.8 = 1.9V$

Calculation of R1, $Vh = 2.5uA * R1 = 1.9$

$$R1 = 760kOhm$$

Calculation of R2,

$$R2 = \frac{1.228*(R1+R2)}{R2} + 2.5uA * R1 \quad (14)$$
$$R2 = 200kOhm$$

IV. SIMUALTION ANALYSIS

The proposed topology resolver-based PMSM motor controller operates at 6000rpm and requires 48VDC. It is made up of the LT8302 fly back converter, a voltage follower circuit for detecting DC and phase voltage, and a voltage comparator circuit for overcurrent and overvoltage to reset the microcontroller. The simulation is shown below.

A. Fly back converter (LT8302)

Fly back converter that will function as a buck-boost converter. The fly back converter converts 12V

to 15V with a load current of 400mA and a load resistance of 37.5Ohm. This converter is also known as an auxiliary power supply. The simulation of the fly back converter is presented in Fig 5.

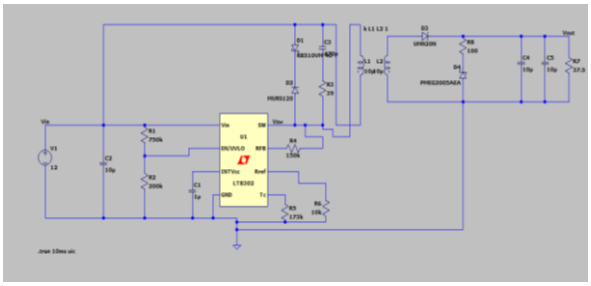

Fig5 simulation of the fly back converter

The UVLO pin will have a voltage of 2.588V. If the voltage at pin point is less than 1.03V, the fly back regulator IC will not function, hence the voltage at pin point will be more than 1.03V. The simulated waveform is depicted in Fig 6.

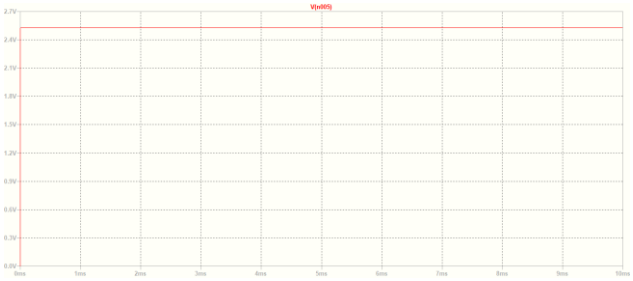

Fig6 waveform of the UVLO voltage

Input voltage 12V applied to the Fly back converter with duty ratio of the 60%. The output voltage and output current of 15V and 400mA. Simulated waveform of the output voltage and current as shown in the Fig 7.

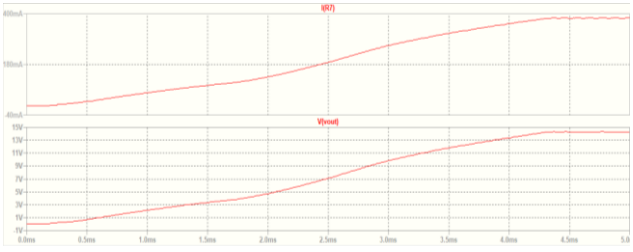

Fig7 waveform of the output voltage and output current

During the discontinuous conduction mode (DCM), the voltage ripples will settle down to begin the next cycle. This will emerge across the switch pin point during no load conditions, and the frequency under this pin will be more than 302kHz, as illustrated in the simulated waveform in fig 8.

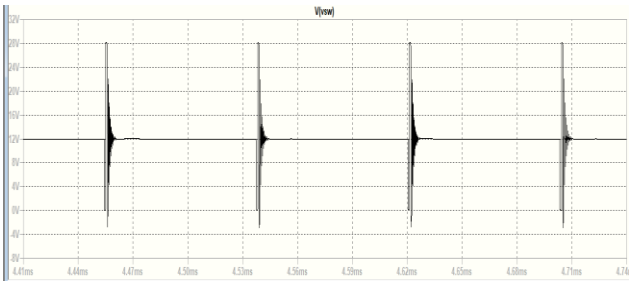

Fig8 voltage waveform at switch during DCM

During the continuous conduction mode (CCM), the load current was 400mA with a load resistance of 37.5 Ohm. During this mode, the leakage voltage will occur across the primary inductance, and the frequency of the switch point will be 320kHz, with the simulated waveform given in Fig 9.

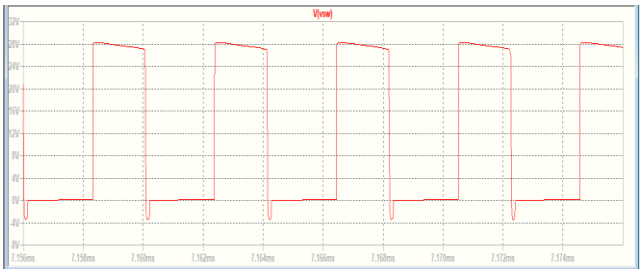

Fig9 voltage waveform across the switch during CCM

B. Simulation circuit used to measure the DC and phase voltage of the power board

DC voltage is applied across the inverter circuit and converted into AC voltage. The AC voltage is measured in terms of phase voltage. DC voltage and phase voltage from the inverter's input and output were fed into voltage follower circuits, which clipped the higher voltage to 5V. The simulated circuits for sensing voltage deliver signals to the microcontroller, as shown in Fig 10.

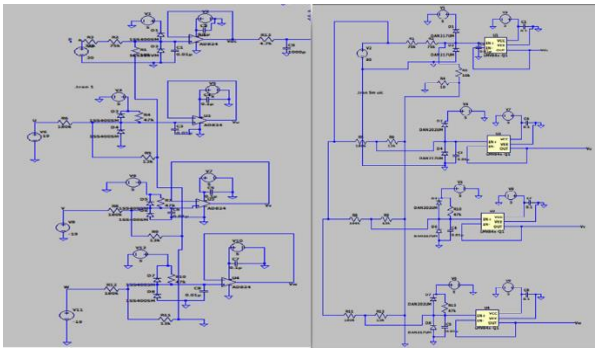

Fig10 simulation circuits for the phase and line voltage measurements

When DC voltage is provided to the inverter circuits. The voltage sensor measures the DC voltage across the inverter input and feeds it to the voltage divider circuits, where it is decreased to less than 5V. The voltage follower circuits will produce the same voltage across their non-inverting terminals and their outputs. Simulated circuits for the two conditions depicted in Fig 10.

When a DC voltage of 30 V is applied across the inverter circuits. The voltage in non-inverting and voltage divider circuits will be 1.875 volts. The voltage at the output of the voltage follower circuits will display as 1.875V. The waveform shown in the fig 11.

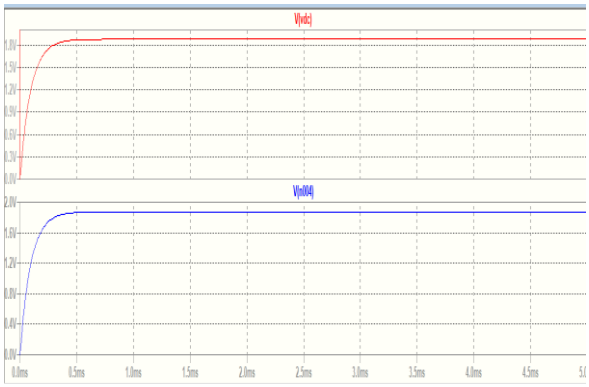

Fig11waveform for the measurement of DC voltage less than 30V.

When the DC voltage delivered to the inverter exceeds 80V, the voltage across the voltage divider and non-inverting terminal of the voltage follower circuit is greater than 5V. The voltage follower circuit operates at 5V, hence the voltage at the non-inverting terminal will be greater than 5V and then clipped to 5V. Sends the voltage level to the microcontroller. The simulated waveform is presented in fig 12.

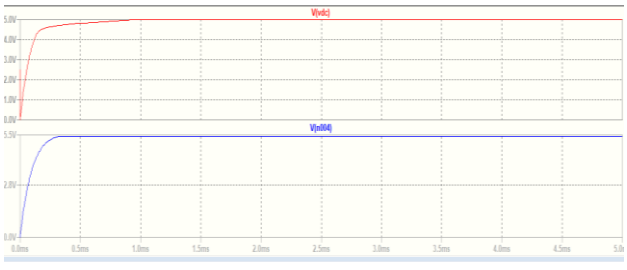

Fig12 waveform for the measurement of DC voltage more than 80V

When a DC voltage is applied to the inverter input, it is converted to an AC voltage and the phase voltage of the inverter's output is measured for each leg. For analysis, a different voltage is delivered across the inverter leg of the voltage follower circuits, and the converted voltage signal is sent to the voltage comparator circuits to reset the microcontroller. The various criteria are discussed below.

When 75V is put across any one inverter leg, the voltage between the voltage divider circuits and non-inverting terminals of the voltage follower circuits is 5.05V. The voltage follower circuits are clipped into 5V, and the waveform is illustrated in Figure 13.

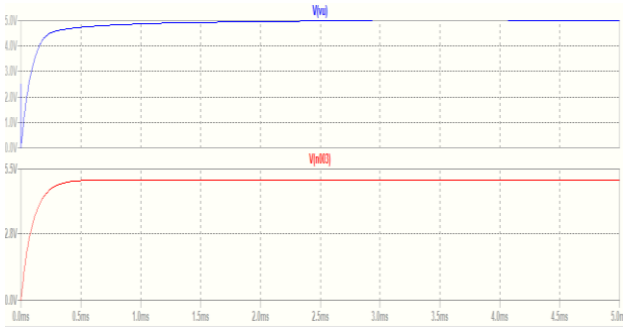

Fig13 output voltage of the follower circuit when the input voltage of 75V

When 0V is supplied across any one inverter leg, the voltage between the voltage divider circuits and the non-inverting terminal of the voltage follower circuits is 1.0253V. The voltage follower circuits send a voltage of 1.0253V to the voltage comparator circuits and waveform illustrated in Fig 14.

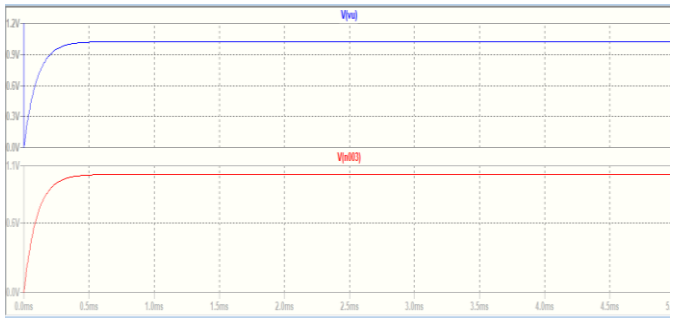

Fig14 output voltage of the follower circuit when the input voltage of 0V

When -19V is applied to any one inverter leg, the voltage appearing across the voltage divider circuits and non-inverting terminals of the voltage follower circuits is 800mV. The voltage follower circuits transmit a voltage of 0V to the voltage comparator circuits and waveform displayed in Fig15.

Fig14 output voltage of the follower circuit when the input voltage of -19V

C. Simulation for over protection (OV) unit

The voltage follower circuits' outputs are used to measure DC voltage. The voltage follower circuits' outputs convey the signal to the voltage comparator circuits. By comparing two distinct voltage levels and sending the signal to the microcontroller. When 5V is put across the voltage divider circuits, the voltage at the non-inverting terminal will be 3.75 V. The DC voltage of the voltage follower circuits will be compared to 3.75 V. If the voltage at the non-inverting terminal (3.75V) is larger than the voltage at the inverting terminal, the voltage difference will be positive, allowing op-amp circuits to raise the voltage level to 5V. The simulated circuits and waveforms are presented in Fig 15 and 16.

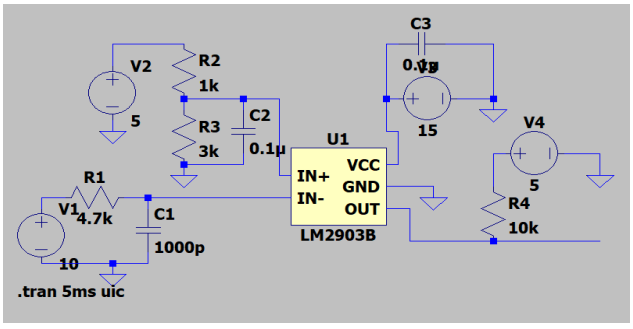

Fig15 simulation circuit for over voltage protection

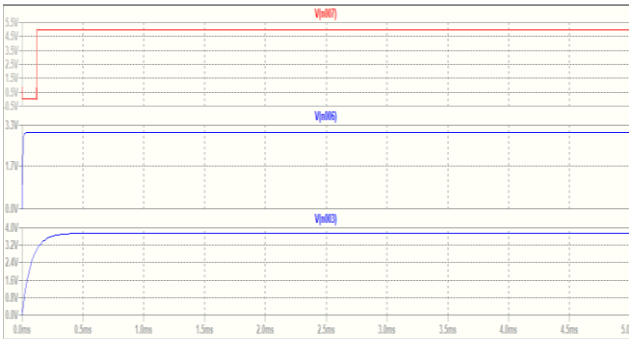

Fig16 simulation waveform does not reset the MCU

When 5V is put across the voltage divider circuits, the voltage at the non-inverting terminal will be 3.75 V. The DC voltage of the voltage follower circuits will be compared to 3.75 V. If the voltage at the non-inverting terminal (3.75V) is less than the voltage at the inverting terminal, the voltage difference will be negative, and the op-amp circuits will pull the voltage level down to 0V. The simulated circuits and waveforms are illustrated in Fig 17.

Fig17 simulation waveform reset the MCU

D. Simulation for over current (OC) protection unit

The output current of the inverter circuits is measured in terms of voltage using the current sensor. The output voltage of the U, V, and W legs is compared to the voltage levels of 4.5V and 500mV. If one of the voltage comparator circuits has a negative voltage difference, the microcontroller should be reset, and vice versa. The simulation circuits are presented in Fig 18.

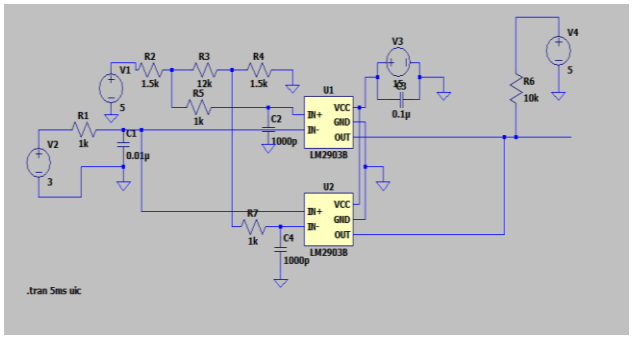

Fig18 simulation circuit for the over current

The voltage of each leg will be compared to the non-inverting terminal voltage of 4.5V and the inverting terminal voltage of 500mV. If the voltage difference is positive, the op-amp will pull up to 5V without resetting the MCU. The waveform depicted below in Fig 19

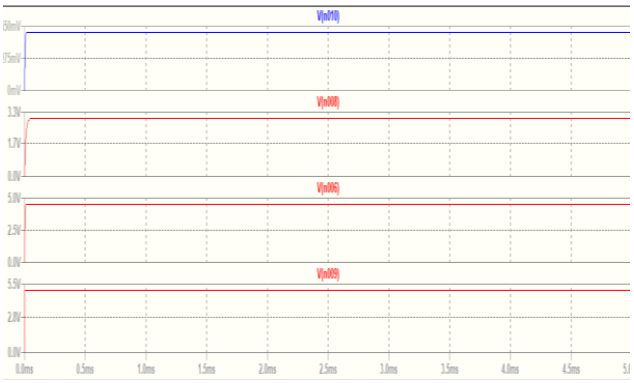

Fig19 waveform for the OC test which pull up to 5V

The voltage of each leg will be compared to the non-inverting terminal voltage of 4.5V and the inverting terminal voltage of 500mV. If the voltage difference is negative, the op-amp will be pulled down to 0V, resetting the MCU. The waveform illustrated below Fig 20.

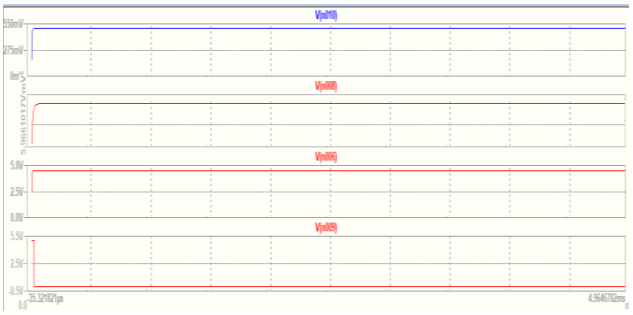

Fig20 waveform for the OC test which will be reset the microcontroller

E. Simulation for the gate driver circuits

When a +15V input voltage is provided to the fly back converter, it converts the output voltage to +15V with a duty ratio of 50% and a load current of 250mA. The fly back converter's input and output voltage are applied to the pulse width modulation (PWM) IC UCC27211. Rectangular PWM pulses are applied to the PWM IC at a frequency of 10kHz, with a dead time of 1500ns, rise time of 1ns, fall time of 1ns, and duty ratio of 50%. The simulated circuit diagram is depicted in Fig 21.

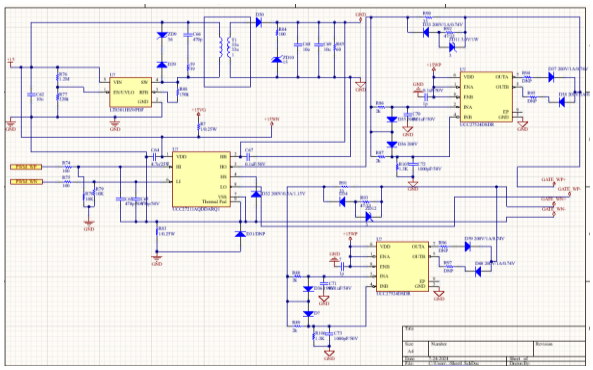

Fig21 simulation circuit of the gate driver circuit

When the PWM pulses applied to UCC27211 with an amplitude of the 5V. PWM IC which operating the voltage level of 15V and pull up the PWM pulses to 15V as shown in the Fig 22.

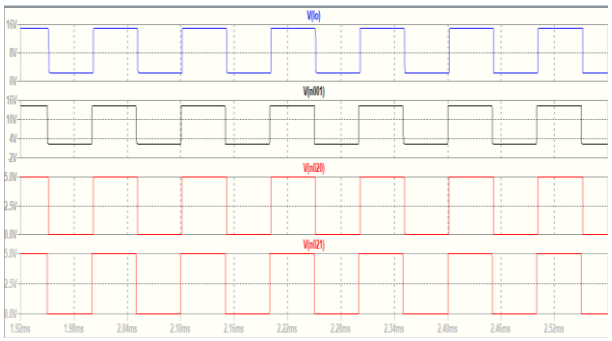

Fig22 PWM pulses generated for UCC27211 IC

The PWM pulses generated by the UCC27211IC are sent to the UCC27524 IC, which pulls the PWM pulses up to 12V due to the difference ground, resulting in PWM pulses of 13V to 15V with a 1500ns dead time. The simulated waveform is depicted in Fig 23.

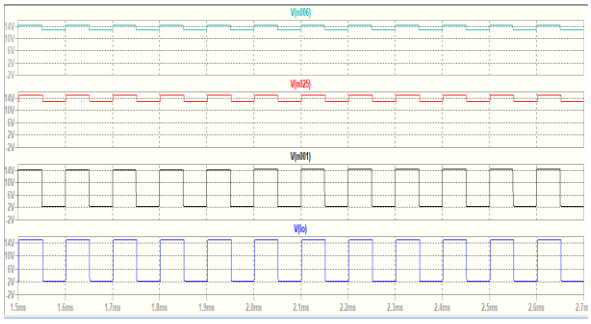

Fig23 PWM pulses generated by the UCC27524 IC

F. Simualtion result

PWM pulses are generated using gate driver circuits supplied to the power board (inverter circuits)

to power the PMSM motor. The feedback from the PMSM motor's silver section will be used to modify the position of the PMSM motor controller. Table III shows a tabulation of the motor running at various speeds, together with the torque and power consumed by the PMSM motor.

Table III Requirement based on the simulation

Motor speed (rpm)	Motor torque (Nm)	Motor power (kW)
100	23.02	0.70
500	22.55	3.48
1000	22.4	6.93
1500	22.29	10.42
2000	21.86	13.82
2500	18.37	17.09
3000	13.36	14.48
3500	13.33	9.07
4000	11.38	5.48

V. CONCLUSION

The simulation of the design and development of a resolver-based PMSM motor controller is shown. The research shows that the motor control unit used full load power at a speed of 4000rpm and a torque of 11.38Nm was achieved. Resolvers and encoders detect the physical operational parameters of equipment in use. They typically measure the speed, position of the shaft, and direction of rotation of the rotor. I simulated the overvoltage, overcurrent, and gate driver circuits. Generated the waveforms for each topology under various situations.

ACKNOWLEDGMENT

I deeply express my sincere gratitude to my guide Dr. S G Srivani, Associate professor, Dept. of EEE, RVCE, Principal and HOD, Dept. of EEE, RVCE and panel members for their valuable guidance throughout the project. I would also like to express my deepest appreciation to Takumi motion controls pvt.ltd, Bengaluru for providing me an opportunity to carry out the project in their organization and help me to gain hands on experience about the project.

REFERENCES

[1] L. Cinti, C. Contò and N. Bianchi, "A Comparison between Hybrid Excited Permanent Magnet and Wound Rotor Motor," *2022 International Symposium on Power Electronics, Electrical Drives, Automation and Motion (SPEEDAM)*, Sorrento, Italy, 2022, pp. 14-19, doi: 10.1109/SPEEDAM53979.2022.9842232.

[2] S. Wang, D. Peng and Z. Wu, "Embedded Position Detection for Permanent Magnet Synchronous Motor with Built-In Magnets," in *IEEE Sensors Journal,* vol. 19, no. 21, pp. 9818-9825, 1 Nov.1, 2023, doi: 10.1109/JSEN.2023.2928336.

[3] A. Deep, N. K. Pilli, A. K. Chauhan and S. K. Singh, "Design and development of rapid prototype controlled PMSM drive," *2022 IEEE IAS Joint Industrial and Commercial Power Systems / Petroleum and Chemical Industry Conference (ICPSPCIC)*, Hyderabad, India, 2022, pp. 134-139, doi: 10.1109/CICPS.2022.7974065.

[4] K. A. Gore and R. T. Ugale, "Design and Comparative Analysis of PMSM, BLDC, SynRM, and PMAssi-SynRM Motors for Two-Wheeler Electric Vehicle Application," *2022 IEEE Conference on Interdisciplinary Approaches in Technology and Management for Social Innovation (IATMSI)*, Gwalior, India, 2022, pp. 1-6, doi: 10.1109/IATMSI56455.2022.10119363.

[5] J. You, P. Wang, Z. Liu and D. Jiang, "Vibration Analysis of Permanent Magnet Synchronous Motors Considering Rotor Position Error Caused by Resolver Static Eccentricity," *2023 IEEE 2nd International Power Electronics and Application Symposium (PEAS)*, Guangzhou, China, 2023, pp. 2348-2352, doi: 10.1109/PEAS58692.2023.10395452.

[6] S. Gupta, S. George and V. Awate, "PI Controller Design and Application for SVPWM Switching Technique Based FOC of PMSM," *2023 Second International Conference on Trends in Electrical, Electronics, and Computer Engineering (TEECCON),* Bangalore, India, 2023, pp. 172-177, doi: 10.1109/TEECCON59234.2023.10335784.

[7] R. Lajić and P. Matić, "Digital Position Control System with a BLDC Motor Using Field Oriented Control," *2023 22nd International Symposium INFOTEH-JAHORINA (INFOTEH)*, East Sarajevo, Bosnia and Herzegovina, 2023, pp. 1-6, doi: 10.1109/INFOTEH57020.2023.10094070.

[8] Aditi, S. Pandey, P. Kumar and M. Sreejeth, "Analysis of Advanced Speed Control Methods for PLC-based Induction Motor Drive," *2021 International Conference on Recent Trends on Electronics, Information, Communication & Technology (RTEICT)*, Bangalore, India, 2021, pp. 610-614, doi: 10.1109/RTEICT52294.2021.9573894.

[9] A. Srivastava, R. Padgil, A. Gupta, A. Lohia and N. P. Nair, "Model-Based Sensored Field Oriented Control Implementation for Permanent Magnet Synchronous Motor," *2021 International Symposium of Asian Control Association on Intelligent Robotics and Industrial Automation (IRIA)*, Goa, India, 2021, pp. 337-344, doi: 10.1109/IRIA53009.2021.9588787.

[10] R. Gora, R. Biswas, R. K. Garg and U. Nangia, "Field Oriented Control of Permanent Magnet Synchronous Motor (PMSM) Driven Electric Vehicle and Its Performance Analysis," *2021 IEEE 4th International Conference on Computing, Power and Communication Technologies (GUCON)*, Kuala Lumpur, Malaysia, 2021, pp. 1-6, doi: 10.1109/GUCON50781.2021.9573814.

[11] S. K. Sethuraman and M. G. Saravanan, "Microcontroller based PWM strategies for the real-time control and condition monitoring of AC drives," *1993 Sixth International Conference on Electrical Machines and Drives (Conf. Publ. No. 376)*, Oxford, UK, 1993, pp. 400-405.

[12] H. Yu, "PWM regulation based on microcontroller control," *2022 International Conference on Electronics and Devices, Computational Science (ICEDCS)*, Marseille, France, 2022, pp. 34-36, doi: 10.1109/ICEDCS57360.2022.00014.

[13] A. M. Aljehaimi and A. A. Alrimali, "Speed Control of IPSMS Using Space Vector PWM," *2023 IEEE 3rd International Maghreb Meeting of the Conference on Sciences and Techniques of Automatic Control and Computer Engineering (MI-STA)*, Benghazi, Libya, 2023, pp. 111-116, doi: 10.1109/MI-STA57575.2023.10169536.

[14] K. V. V. Satyanarayana, K. B. Shah and V. P. Chandran, "Speed Control of Multicarrier PWM Based 11-Level Inverter Fed Induction Motor Drive," *2021 5th International Conference on Electrical, Electronics, Communication, Computer Technologies and Optimization Techniques (ICEECCOT)*, Mysuru, India, 2021, pp. 562-568, doi: 10.1109/ICEECCOT52851.2021.9708009.

[15] Qiang Li, Hai Huang and Binchuan Yin, "The study of PWM methods in permanent magnet brushless DC motor speed control system," *2008 International Conference on Electrical Machines and Systems*, Wuhan, 2008, pp. 3897-3900.

[16] S. Kotabagi, R. Nayak, S. Dalabanjan, V. P. N, P. L. Patil and S. Hemadri, "Maximum Power Point Tracking using Buck-Boost converter for EH-PMIC," *2023 36th International Conference on VLSI Design and 2023 22nd International Conference on Embedded Systems (VLSID)*, Hyderabad, India, 2023, pp. 1-6, doi: 10.1109/VLSID57277.2023.00052.

[17] S. Kotabagi, R. Nayak, S. Dalabanjan, V. P. N, P. L. Patil and S. Hemadri, "Maximum Power Point Tracking using Buck-Boost converter for EH-PMIC," *2023 36th International Conference on VLSI Design and 2023 22nd International Conference on Embedded Systems (VLSID),* Hyderabad, India, 2023, pp. 1-6, doi: 10.1109/VLSID57277.2023.00052.

[18] A. Liyanage, M. Nagrial, A. Hellany and J. Rizk, "Speed Control of Induction Motors Using V/f Control Method," *2022 International Conference on Electrical and Computing Technologies and Applications (ICECTA)*, Ras Al Khaimah, United Arab Emirates, 2022, pp. 424-429, doi: 10.1109/ICECTA57148.2022.9990374.

[19] S. Sakunthala, R. Kiranmayi and P. N. Mandadi, "A study on industrial motor drives: Comparison and applications of PMSM and BLDC motor drives," *2017 International Conference on Energy, Communication, Data Analytics and Soft Computing (ICECDS)*, Chennai, India, 2017, pp. 537-540, doi: 10.1109/ICECDS.2017.8390224.

[20] A. Mondal, J. Khan, S. Prins and K. S., "Control of Dual Motor Test Bench for Performance Testing of PMSM for Traction Application," *2023 IEEE Silchar Subsection Conference (SILCON)*, Silchar, India, 2023, pp.

1-6, doi: 10.1109/SILCON59133.2023.10404719.

[21] A. M. Lulhe and T. N. Date, "A design & MATLAB simulation of motor drive used for electric vehicle," *2015 International Conference on Control, Instrumentation, Communication and Computational Technologies (ICCICCT)*, Kumaracoil, India, 2015, pp. 739-743, doi: 10.1109/ICCICCT.2015.7475378.

[22] S. S. Rauth and B. Samanta, "Comparative Analysis of IM/BLDC/PMSM Drives for Electric Vehicle Traction Applications Using ANN-Based FOC," *2020 IEEE 17th India Council International Conference (INDICON)*, New Delhi, India, 2020, pp. 1-8, doi: 10.1109/INDICON49873.2020.9342237.

[23] R. R. Chowdhury and G. Koperundevi, "Motor Selection and Performance Assessment of SUV Electric Mobility Employing Indian Roads," *2022 IEEE 10th Power India International Conference (PIICON)*, New Delhi, India, 2022, pp. 1-6, doi: 10.1109/PIICON56320.2022.10045308.

[24] A. M. Lulhe and T. N. Date, "A technology review paper for drives used in electrical vehicle (EV) & hybrid electrical vehicles (HEV)," *2015 International Conference on Control, Instrumentation, Communication and Computational Technologies (ICCICCT)*, Kumaracoil, India, 2015, pp. 632-636, doi: 10.1109/ICCICCT.2015.7475355.

[25] D. S. Yadav and M. Manisha, "Electric Propulsion Motors: A Comparative Review for Electric and Hybrid Electric Vehicles," *2022 IEEE International Conference on Distributed Computing and Electrical Circuits and Electronics (ICDCECE)*, Ballari, India, 2022, pp. 1-6, doi: 10.1109/ICDCECE53908.2022.9793099.